Elucidating Challenges of Reactions with Correlated Reactant and Product Binding Energies on an Example of Oxygen Reduction Reaction

Ted H. Yu[1,2]*, *Randy Torres*,[1] *Boris V. Merinov*,[2*] *William A. Goddard*,[2]

[1]Department of Chemical Engineering, California State University, Long Beach, California, 1250 Bellflower Blvd, Long Beach California, 92840, USA.

[2]Materials and Process Simulation Center, California Institute of Technology, 1200 East California Blvd., m/c 139-74, Pasadena, California 91125, USA

Abstract

Using density functional theory (DFT), Pt-based sandwich catalysts have been studied to identify a strategy for improving the energetically unfavorable O hydration catalytic reaction ($O + H_2O \rightarrow 2OH$) in fuel cells. The challenge for this type of reaction is that the reactant, O, and product, OH, have correlated binding energies, making the improvement of the overall energetics of the reaction problematic. We screened 28 different transition metals as the Pt-M-Pt sandwich middle layer and developed a new index that specifically describes the difficulty of the reaction which involves adsorbed atomic O as the reactant and adsorbed OH as the product. This index is found

to predict well the barrier of the O hydration. In order to understand how the index can be optimized, we further studied the electronic density of states (DOS) to elucidate the DOS changes for the different Pt-M-Pt sandwiches. This gives insight on strategies that might be applied to improve the catalytic reactions where the reactant and product have correlated binding energies, which is in fact a common challenge in heterogeneous catalysis.

KEYWORDS: ORR, catalysis, DFT, density of state, fuel cells

1. INTRODUCTION

Heterogeneous surface catalysis facilitates conversion of reactants to products. The overall reaction consists of individual reaction steps. The rate of each step and the overall reaction is significantly related to the binding energy of the reactant and product. A possible strategy for searching advanced catalytic surfaces may involve matching the binding energy for each reaction step, so that the largest, rate-determining barrier would be minimized. In this way, it would be ideal to tailor a catalyst that has an ideal binding energy for each species along the mechanism, and the overall mechanism contains as little “bumps along the road” as possible.

The common problem when researching an ideal catalyst, especially for multistep reactions, is that the intermediate species often have correlated binding energies. Selecting a catalyst that lowers or raises the binding energy of a particular intermediate may also lower or raise the binding energy of other intermediates (correlated binding energies). In this case, it will not improve a particular reaction step, since the binding energy of the product and reactant changes by the same amount, resulting in the same overall energy of reaction (ΔE). Thus, new strategies need to be developed that would allow changing the binding energy of a particular intermediate without affecting the others in order to improve the individual reaction steps. The key here is to

figure out ways to make the binding energies of intermediates that were previously correlated to become non-correlated.

An example of a well-studied reaction with correlated binding energies is the oxygen reduction reaction (ORR) in a proton-exchange membrane fuel cell (PEMFC). The ORR adsorbed intermediates, such as O and OH, have correlated binding energies[1, 2], which makes it difficult to improve the efficiency of this reaction. We further examine this reaction to identify strategies for improving ORR catalysts.

The ORR can be broken down into eight fundamental reaction steps:[1, 3, 4]:

1) H_2 dissociation: $H_{2ad} \rightarrow 2H_{ad}$
2) O_2 dissociation: $O_{2ad} \rightarrow 2O_{ad}$
3) Direct OH formation: $O_{ad} + H_{ad} \rightarrow OH_{ad}$
4) O hydration: $O_{ad} + H_2O_{ad} \rightarrow 2OH_{ad}$
5) OOH formation: $O_{2ad} + H_{ad} \rightarrow HOO_{ad}$
6) OOH dissociation: $OOH_{ad} \rightarrow OH_{ad} + O_{ad}$
7) H - OOH dissociation: $HOO_{ad} + H \rightarrow 2OH_{ad}$
8) H_2O formation: $OH_{ad} + H_{ad} \rightarrow H_2O_{ad}$

By including these fundamental steps into an overall ORR mechanism, we distinguish three chemical processes:

I. O−O bond activation, which can occur via two reactions: O_2 dissociation (2) or OOH formation (5) followed by OOH dissociation (6)
II. OH formation proceeds via three reactions: Direct OH formation (3), O hydration (4), or H−OOH dissociation (7).
III. H_2O Formation: There is only one reaction (8).

Earlier we found that the O hydration step[4] in process II (OH formation) is probably the rate-determining step (RDS) for the ORR on Pt in solution with a barrier of 0.50 eV. O hydration has a lower barrier than direct OH formation ($O_{ad} + H_{ad} \rightarrow OH_{ad}$) for pure Pt, making it the more relevant reaction to study. In the case of Pt alloys when the surface is 100% Pt but the second layer is not, the O hydration barrier was lower than direct OH formation (0.34 eV vs. 0.57 eV for Pt_3Ni)[3]. Therefore, O hydration is the more relevant reaction to study for the case of Pt-M-Pt sandwiches due to the 100% Pt surface which has shown a preference for O hydration over direct OH formation. It has been observed in experiments by Ertl et al[5, 6] and Campbell et. al[7]. It was also shown that the reactant, O_{ad}, dominates as the adsorbed intermediate above 0.7V, while OH_{ad} dominates below[8, 9], making this reaction more relevant at desirable potentials. This reaction does not have H_{ad} as a reactant, which makes it independent of potential. Calculations of potential dependent barriers require computationally expensive methods or complicated schemes that involve approximations of redox reactions and/or charged periodic systems[10-14]. This makes the O hydration step, an ideal barrier to focus on, as it is an experimentally relevant reaction that can be determined accurately.

The barriers for process I and III of the ORR connect well with the binding energy, whereas the process II shows poor coupling for pure metals due to the correlated binding energies[1, 2] of the reactant (O) and product (OH). In our previous paper[1], we showed for very noble metals (Ag, Au), process I (O−O bond activation) is rate-limiting due to the large binding energy of the product (atomic O) compared to the reactant (O_2). On the other hand, for easily oxidized metals (Cu, Ir, Rh, Ni, Os, Ru, Co, Fe), process III (H2O formation) is rate-limiting due to the large binding energy of the reactant (OH) compared to the product (H_2O). Process II is rate-limiting for Pt, because it has intermediate binding energy which makes both Process I and Process III

very fast. Although Pt is the best pure metal catalyst for ORR, it can still be improved further by alloying it with metals in the 2nd layer that affect the binding characteristic of the surface Pt, so that Process II becomes faster.

As shown previously, the degrees of oxo-philiciity (relative binding energy of O and OH) of pure metal catalysts are similar and their binding energies have been demonstrated to scale linearly. It is desirable to find an oxo-asymmetry index that specifically predicts the difficulty of process II. In this way, each of the three processes of the ORR can be improved by focusing on the following criteria:

- O_2 activation: High O binding energy.
- OH formation: High oxo-asymmetry index
- H_2O Formation: Low OH binding energy.

We have tested our hypothesis on 28 Pt-M-Pt (M is a transition metal) sandwich catalysts which consist of Pt on the surface layer, a transition metal in the second, and Pt in the bulk. Such catalysts display unique properties that improve the sluggish ORR in fuel cells.[15, 16] It was shown for Pt-M-Pt (M = Ru, Rh, Pd, Re, Os, Ir, Pt) that the O and OH binding energies could possibly be non-correlated for these materials.[1, 17] Thus, we seek to find cases of high oxo-asymmetry, and this class of catalysts was shown to display this property. In our previous work, we also found that a position of the surfface d-band center poorly estimates the binding energy of O and OH on pure metal surfaces.[1] Here, we would like to determine how well the d-band center correlates with the binding energy for the 28 Pt-M-Pt sandwiches.

2. COMPUTATIONAL METHODS

Periodic QM calculations were carried out using the SeqQuest code[18, 19] which employs Gaussian basis functions at the optimized double-ζ plus polarization level (rather than the plane-

wave basis often used in periodic systems). We use DFT with the Perdew-Burke-Ernzerhof[20] (PBE) approximation of the generalized gradient approximation[21] (GGA) exchange-correlation functional. The up-spin orbitals are allowed to be optimized independently of the down-spin orbitals (spin-unrestricted DFT). The small core pseudopotentials with angular momentum projections are applied in our calculations.

The DOS structures were analyzed using the SeqQuest post-analysis code.[19] The bands are further broadened by convolution with a 0.5 eV FWHM Gaussian function to approximate the experimental Gaussian broadening and Lorentzian lifetime broadening. We applied the Nudged Elastic Band[22] (NEB) function of SeqQuest to calculate energy barriers of the intermediate reactions for the best and worst Pt-M-Pt sandwiches as determined by the index.

The calculated lattice parameter (3.97 Å) of the bulk Pt was used for all 28 Pt-M-Pt sandwiches. Surfaces are modeled as two-dimensional infinite periodic slab with four atoms per cell. The thickness of the slabs were three, four, or five layers with the top two layers relaxed. For the three slabs, the energy convergence was tested against thicker slabs to see that it was sufficient. Because of the Gaussian basis functions, a vacuum layer is not necessary for two-dimensional calculations. The real space grid density is 5 points per angstrom while the reciprocal space grid is 5x5x0. The coverage for atomic O is 0.25 ML following experimental results[23]. The initial state of O hydration is 0.25 ML coverage atomic O with 0.25 ML coverage water co-adsorbed. The 0.50 ML OH coverage of the final O hydration state corresponds to the experimental coverage of 0.67 ML[24].

RESULTS AND DISCUSSIONS

Based on the binding energies (BE) of our previous calculations on pure metal surfaces (Fe, Co, Ni, Cu, Ru, Rh, Pd, Ag, Os, Ir Pt, Au),[2] an oxo-symmetry linear dependence, $BE_{OH} = 0.667 \cdot BE_O$

– $8.17 \cdot 10^{-4}$, might be proposed to best fit the O and OH binding energies of these metals. Since the barrier for the OH formation does not vary with different pure metals[4], the line plotted for the twelve pure metals with BE_O as the x-axis and BE_{OH} as the y-axis, is the baseline for correlated binding behavior of pure metals. This line is a combination of both the O and OH binding energy difference ($BE_O - BE_{OH}$) and ratio (BE_O/BE_{OH}). The small $8.17 \cdot 10^{-4}$ eV y-intercept shows that the BE_O/BE_{OH} ratio is the dominant correlation. To measure the degree of non-correlated O/OH binding energy in the Pt-M-Pt sandwiches, we plotted the O and OH binding energies of each Pt-M-Pt sandwich (Figure 1 and Table 1) to determine how far it is from the line for the pure metals. From Figure 1, we can conclude that the previously observed non-correlated O and OH bindings for some Pt-M-Pt sandwich catalysts[1, 17], are not a universal trend. Although there exist several catalysts that are far from the main line, the general trend is that the O and OH binding energies of all 28 Pt-M-Pt sandwich catalysts average out to the main line. This differs from our previously published result that compared just seven Pt-M-Pt sandwich catalysts with Pt-group metals (Ir, Os, Pd, Pt, Re, Rh, Ru) in the center layer[2] for which we observed an X-crossing non-correlated binding line to the main line. However, this trend does not extend to all transition metals, if comparing a larger group beyond just the Pt-group metals. As explained[17], the inverse scaling exceptions to the d-band model are related to non-negligible Pauli repulsion for systems containing the latter transition metals not including the 3d's (Au, Ag, Cu).

We use the pure metal centerline in Figure 1 to create an index that estimates how well a catalyst will perform for process II, OH formation, of the ORR. This process can be realized via two reactions: direct OH formation or O hydration[4] The new index is the perpendicular distance from the pure metal line and an indicator of the exothermicity of reactions starting with O and ending with OH. The reason for not using the exothermicity explicitly, such as $BE_O - BE_{OH}$, is

that they are very different for pure metals; for example, this value is 0.61 eV for Au and 1.74 eV for Fe.[1] Unlike processes I and III, process II does not have any direct correlation to binding energy as shown in our previous work.[1] Therefore, the assumption is to set this pure metal centerline as the basis for comparing other catalysts to estimate process II. The index is determined by the following equation:

$$\textit{oxo-asymmetry index} = f\,(BE_{OH}, BE_O) = -10 \cdot BE_O + 15 \cdot BE_{OH} + 1.2 \cdot 10^{-3} \qquad (1)$$

The index is very positive for catalysts which fall to the upper left of the centerline, while it is very negative for those falling to the lower right of the centerline. Pt-W-Pt was found to have the best index value, 6.97, and Pt-Ag-Pt has the worst index value, –5.82.

To see how this index correlates with the energetics of the O hydration reaction, we calculated the NEB barrier for this reaction on all 28 Pt-M-Pt catalysts, with the barriers of Pt-Ag-Pt, Pt-W-Pt, and pure Pt catalysts shown in Figure 2. As expected, Pt-Ag-Pt has a barrier much higher than Pt (0.68 vs. 0.24 eV), while Pt-W-Pt has a barrier much lower than Pt (0.12 vs 0.24 eV). From Figure 1, both Pt-W-Pt and Pt-Ag-Pt have the O binding energy of about 3.5 eV, but their OH binding energy differs by almost 1 eV. This demonstrates that there exist cases where the binding energies of O and OH become non-correlated which may help improve such reactions as process II of the ORR. Application of the index can be extended to intermediates of other reactions, such as nitrogen hydrogenation.[25] This multi-step reaction can have up to seven N_xH_y intermediates as N_2 is converted to NH_3. It may be improved, if it would be possible to uncorrelate the binding energies of the corresponding intermediates.

The NEB barrier for O was plotted against each respective index value for all 28 Pt-M-Pt catalysts. Since the index is a measure of the difference/ratio of the binding energy of the

reactant (O) and product (OH), there should also be a relationship to the barrier, which was confirmed in Figure 3.

The next step is to analyze how the binding energies of O and OH are uncorrelated for the different Pt-M-Pt sandwich catalysts. The bond between the Pt-M-Pt sandwich and O/OH is formed due to the interaction of the d-DOS of the surface Pt atoms with the p-DOS of the oxygen atom in O or OH molecules (p-DOS is p-orbital density of state not to be confused with PDOS, partial density of state).[26] The d-DOS of the surface Pt can be modified by subsurface transition metal atoms. A simple way to see how the d-DOS is modified is to look specifically at the d-band center of the surface Pt, and how it changes with different subsurface atoms.[27] The d-band center is defined as $E_d - E_F$, where E_d is the energy of the average occupied d-electron density and E_F is the Fermi energy. In the simplest version of this model, O and OH binding energies are correlated because a d-band closer to the Fermi level will more empty in anti-bonding states above the Fermi level, forming a stronger bond with both O and OH.

We find that the d-band center position correlates better to the index than to the OH or O binding. Figure 4a shows a plot of the index vs. the d-band center, while Figures 4b and 4c represent plots of the binding energy vs. the d-band center for O and OH, respectively. The linear fit has a positive slope for the O binding vs. the d-band center, and a negative slope for the OH binding vs. the d-band center. This agrees with previously published results[17] that show the unique negative correlation between the d-band center and OH binding. However, the R^2 value for these previous results are very poor, 0.1218 and 0.0541 for O and OH, respectively. If we limit the center metal to the cases compared in the paper by Menning et al (Ti, V, Cr, Mn, Fe, Co, Ni, Pt) for the comparison of d-band center and O binding, the linear fit R^2 improves from 0.1218 to 0.6521, as shown in Figure 4b. Similarly, if we limit the center metal to row 5-6,

columns 6-10 to observe negative correlation trend[17] (Mo, Tc, Ru, Rh, Pd, W, Re, Os, Ir, Pt), the R^2 for d-band center vs. OH binding improves to from 0.0541 to 0.8542 as shown in figure 4c.

Thus, the lack of linear fit for the binding energy vs. d-band center plot may be attributed to the larger set of different Pt sandwiches studied, 28, compared to the previous studies.[16, 17] The poor linear correlation between the O binding and d-band center might be explained that the d-band center is just a very general indicator amongst many others that contribute to the binding energetics. It was also shown previously[1] that for pure metals, the linear fit between d-band center and binding energy depended highly on the type of DFT used, with poor linear fit resulting when PBE was used[1, 15].

Another useful indicator mentioned is the d-DOS within 0.25 eV of the Fermi level.[15] However, the problem with this indicator for non-Pt metals is that it does not explain the strong O/OH binding energy of pure Cu, which has no d-density at the Fermi energy[1, 28]. From the computation viewpoint, the d-DOS can be an important tool to describe binding properties[15]. For better conclusions, it is more appropriate to analyze the DOS structure rather than the d-band center location. We examined the specific DOS structure of the best and worst determined case, Pt-W-Pt and Pt-Ag-Pt, respectively, and compared the overlap between these peaks and the molecular p-DOS peaks of atomic O and OH.

In Figure 5, the d-DOS of the Pt-W-Pt (index = 6.97) and Pt-Ag-Pt (index = –5.82) sandwich catalysts are shown (the highest and lowest index value cases). We can see that the Pt-W-Pt d-DOS is shifted more to the left, away from the Fermi energy, compared to that of Pt-Ag-Pt. Since shifting the d-band to the left increases overlap with the OH p-DOS and away from the O p-DOS, Pt-W-Pt has a stronger preference to bind to OH than O, when compared to Pt-Ag-Pt.

Comparing the overlap between the surface Pt d-DOS with the molecular O and OH p-DOS, we conclude that the difference appears because the energy of three of the p-orbitals for O lies between −10 and −12 eV, while four p-orbitals for OH lies between −8 and −3 eV. These OH p-electrons overlap with the d-DOS of the Pt-M-Pt sandwiches. They overlap more in Pt-W-Pt, because its d-density is more down-shifted with d-band filling. It has a deeper d-band center of −3.6 vs. -2.1 eV in Pt-Ag-Pt.

To study this for all 28 cases of Pt-M-Pt catalysts, we define the overlap as the difference in the catalyst's d-DOS overlap with the p-DOS O and OH. As seen in Figure 6, the peaks of the OH p-DOS lie at –5.93, –4.35, –3.77, and –0.67 eV. The only O p-DOS peak that interacts with the catalyst is at –0.27 eV.

$$\text{Overlap} = \text{d-DOS}(-5.93)+\text{d-DOS}(-4.35)+\text{d-DOS}(-3.77)+\text{d-DOS}(-0.67) -\text{d-DOS}(-0.27) \quad (2)$$

The overlap is used to compare all 28 Pt-M-Pt sandwich metals where we found its correlation with the index. This explains why the index correlates well with the d-band center in Figure 4a. It also provides a new signature that both theorists and experimentalists can look at in the d-DOS. The location of the p-DOS of the reactant and the product is shown to relate directly to the relative binding energy of the two. This provides analysis of the catalyst surface DOS beyond one dimension (e.g. with d-band center alone), and provides a basis for multi-dimensional analysis that can improve correlated reactions as well. We also looked at the p-DOS and d-DOS of the bounded O and OH states on the catalyst, but there was not enough coherency to see a trend.

The entire ORR is a balancing act where all three above-mentioned processes (O_2 activation, OH formation and H_2O Formation) need to be simultaneously optimized to minimize the overall

RDS barrier. In Figure 7, we show how this can be accomplished from our plot of the O and OH binding energy for the Pt-M-Pt sandwich catalysts.

We isolated the Pt-M-Pt sandwiches based on three criteria. The first criterion is a high value for the index for easy O hydration. This is represented by the region to the upper left of the O and OH correlated-diagonal line. The second and third criteria are high O binding energy and low OH binding energy values. In order to set what is the minimum O binding energy and maximum OH binding energy, we used our previously calculated binding energies for Pt_3Ni, which shows one of the best reported catalytic activities[29]. First, we plot a horizontal line (within the errors of DFT) corresponding to the OH binding energy of Pt_3Ni. OH binding energies weaker than this fall below this line and will have easy H_2O formation, because OH is the reactant. Similarly, we plot a vertical line for the O binding energy of Pt_3Ni, and binding energies stronger than this energy fall to its right, meaning that O_2 activation is easy because O is the product.

Extremes in strong OH binding energy (BE_{OH} = 5.22 eV for pure Fe) or weak O binding energy (BE_O = 2.42 eV for pure Au)[1] cause the overall ORR to be slow. A careful balance is needed to make all three processes optimal. As seen in Figure 7, a triangle can be built. We consider this triangle as the ideal binding energy area for the ORR catalysts. Only Pt-Ru-Pt falls within this ideal triangle. Pure Pt appears to have a too low oxo-asymmetry index value and appears to be limited in process II as it was shown in our previous work.[3, 4] Pt-Pd-Pt, Pt-Ir-Pt, and Pt-Rh-Pt need to be moved more to the upper left which also means improving process II of the ORR. Pt-Os-Pt needs to be moved more down which means process III, H_2O formation, limits the ORR. Similarly, the catalyst with the highest index value, Pt-W-Pt, has a strong OH

binding energy, making it non-ideal for the H_2O formation. For the Pt-monolayer catalysts, our analysis shows that Ru is the ideal transition metal to be the middle sandwich layer.

Lastly, the effect of potential needs to be considered for the 28 cases we studied. The onset potential for the correlated binding reaction, $O + H^+ + e^- \rightarrow OH$ can be calculated by defining the energy of H^+ by the definition of the standard hydrogen electrode reaction, $H^+ + e^- \rightarrow \frac{1}{2}H_2$, as zero volts[3]. Previous studies have shown that this reaction[3] is the least exothermic of the four electron ORR reaction, making its energy difference the negative of the total onset potential:

1) $Pt\text{-}M\text{-}Pt\text{-}OO + 4H^+ + 4e^- \rightarrow Pt\text{-}M\text{-}Pt\text{-}OOH + 3H^+ + 3e^-$

2) $Pt\text{-}M\text{-}Pt\text{-}OOH + 3H^+ + 3e^- \rightarrow Pt\text{-}M\text{-}Pt\text{-}O + H_2O + 2H^+ + 2e^-$

3) $Pt\text{-}M\text{-}Pt\text{-}O + 2H^+ + 2e^- \rightarrow Pt\text{-}M\text{-}Pt\text{-}OH + H^+ + e^-$

4) $Pt\text{-}M\text{-}Pt\text{-}OH + H^+ + e^- \rightarrow Pt\text{-}M\text{-}Pt + H_2O$

Theoretically, the onset potential of Reaction 3 can be defined as: $E_{M\text{-}O} + \frac{1}{2}E_{H2} - E_{M\text{-}OH}$. Table 2 lists the onset potential for Reaction 3 for all 28 cases, and it is seen that a high index does increase the onset potential for most Pt-M-Pt sandwich catalysts except Pt-Au-Pt and Pt-Ag-Pt. However, care must be made because a high index also leads to a lower onset potential in Reaction 4, because M-OH is now a reactant that is much more stable. To account for this, Table 2 also shows the onset potential for Reaction 4 as defined as: : $E_{M\text{-}OH} + \frac{1}{2}E_{H_2} - E_M - E_{H_2O}$. The third column defines the predicted onset potential as the lower potential of the two. We see that although Pt-W-Pt has the highest index and a highly favorable Reaction 3, its predicted onset potential (0.55 V) is actually lower than that of pure Pt (0.90 V). On the other hand, our recommended catalyst, Pt-Ru-Pt, has a higher predicted onset potential (0.94 V) than Pt.

Comparing with experiments, the only study done on Pt-M-Pt catalysts involves M = 3d transition metals[16] and did not involve Ru. A related study looked at a Pt monolayer on pure Ru

catalyst[30, 31]. The main difference with these catalysts is that the lattice used is Ru (0001), whereas Pt-Ru-Pt catalysts has a lattice of Pt (111). Another major issue facing alloy catalysts is the subject of durability. In this respect, Pt_3Ni and Pt_3Co catalysts suffer from metal leaching during operation[32, 33]. For Pt-Ru catalysts, durability tests have been performed, for its application as an anode catalyst in direct methanol fuel cells[34]. The surface segregation of Pt-Ru catalysts[35, 36] has been studied in the presence of O and OH. Pt-Ru was found to be one of the better alloys in terms of metal leaching to the surface. When comparing the energy of Pt-skin versus Pt-bulk composition for the (111) surface when OH was adsorbed on the surface, Pt-skin was found to be favorable[35] for Pt_3Ru, while it was shown to be unfavorable for Pt_3Ni.

Such an approach can be extended to more complicated multi-step heterogeneous catalytic reactions, where diagrams similar to Figure 6 may help identify the ways of improving each step and the overall reaction. For instance, if a step has correlated binding energies between reactant and product, one should look at the p-DOS of the product and reactant to determine where they overlap with the d-DOS of the catalyst. If a certain catalyst has d-DOS that overlaps particularly well with one reaction specie but not the other, this step can possibly be improved by one of the two ways: 1) changing the surface d-DOS so it overlaps more with the product p-DOS, and 2) changing the surface d-DOS so it overlaps less with the reactant p-DOS. This strategy would be best employed with theory, as the effect of small changes at the atomic level to the d-DOS can be determined faster than with experiments.

3. CONCLUSIONS

This work elucidates the challenges faced when trying to improve a reaction where the reactants and products have correlated binding energies. To study the phenomenon of non-correlated binding, we performed calculations on Pt-M-Pt sandwich catalysts that have been

shown to exhibit this. By creating the specific index that calculates the perpendicular distance of the Pt-M-Pt sandwich catalyst to the best fit line of the O and OH binding energies based on the data generated for a series of pure metals, we have identified Pt-W-Pt as the best and Pt-Ag-Pt as the worst sandwich catalyst for the O→OH reaction. This conclusion is confirmed by our NEB calculation results. However, the ORR can be considered as consisting of three determinative chemical processes: I) O_2 activation, II) OH formation and III) H_2O formation, and to improve the overall reaction, a balancing act of all three processes is required. The index proposed serves as a simple indicator that predicts a possible efficiency of the ORR catalyst. Improving this index involves finding a catalyst that has the d-DOS overlapping well with the p-DOS of the product (OH) but not the reactant (O). Our three criteria are following: large O binding energy, high index, and low OH binding energy. It is practically impossible for a catalyst to satisfy all three criteria, however, we have identified a region where each chemical process might be energetically favorable so that the RDS of the overall ORR would be minimized. We find Pt-Ru-Pt to be the ideal Pt-sandwich catalyst from our analysis. With the understanding of how the DOS positions of the catalyst and the adsorbate relates to the reaction rate, we can tackle more difficult reactions involving multiple intermediate adsorbates, such as nitrogen hydrogenation. Like the d-band center, this is a physical quantity that can be obtained both theoretically and experimentally, which can provide opportunities for future collaborations.

ACKNOWLEDGEMENTS

This work was supported by Ted Yu's CSULB start up grant. Randy Torres was supported by the Hispanic Serving Institution (HSI-STEM) Winter Program, Louis Stokes Alliances for Minority Participation (LSAMP) Scholarship, Sally Cassanova Scholars Program, and the American Chemical Scholars Program. This work was partially supported by the National

Science Foundation (grant CBET-1512759, Caltech). The facilities of the Materials and Process Simulation Center used in this study were established with grants from DURIP-ONR, DURIP-ARO, and NSF-CSEM.

AUTHOR INFORMATION

Corresponding Authors

*E-mail: ted.yu@csulb.edu (T.H.Y.)

*E-mail: merinov@caltech.edu (B.V.M.)

REFERENCES

1. T. H. Yu, T. Hofmann, Y. Sha, B. Merinov, D. J. Myers, C. Heske and W. A. Goddard, J Phys Chem C (117), 26598-26607 (2013).
2. J. K. Nørskov, J. Rossmeisl, A. Logadottir, L. Lindqvist, J. R. Kitchin, T. Bligaard and H. Jonsson, J Phys Chem B **108** (46), 17886-17892 (2004).
3. Y. Sha, T. H. Yu, B. Merinov, P. Shirvanian and W. A. Goddard, J Phys Chem C **116**, 21334-21342 (2012).
4. Y. Sha, T. H. Yu, B. Merinov, P. Shirvanian and W. A. Goddard, Journal of Physical Chemistry Letters **2**, 572-576 (2011).
5. C. Sachs, M. Hildebrand, S. Völkening, J. Wintterlin and G. Ertl, J. Chem. Phys. **116**, 5759-5773 (2002).
6. S. Völkening, K. Bedürftig, K. Jacobi, J. Wintterlin and G. Ertl, Phys. Rev. Lett. **83**, 2672-2675 (1999).
7. W. Lew, M. C. Crowe, E. Karp, O. Lytken, J. A. Farmer, L. ARnadottir, C. Schoenbaum and C. T. Campbell, J Phys Chem C **115**, 11586-11594 (2011).
8. J. X. Wang, J. Zhang and R. R. Adzic, J. Phys. Chem. A **111**, 12702-12710 (2007).
9. J. X. Wang, F. A. Uribe, T. E. Springer, J. Zhang and R. R. Adzic, Faraday Discuss **140**, 347-362 (2008).
10. M. J. Janik, C. D. Taylor and M. Neurock, J Electrochem Soc **156** (1), B126-B135 (2009).
11. X. Nie, E. M.R., M. J. Janik and A. Asthagiri, Angew Chem Int Edit **52**, 2459-2462 (2013).
12. K. Chan and J. K. Nørskov, Journal of Physical Chemistry Letters **6**, 2663-2668 (2015).
13. Y. Sha, T. H. Yu, B. V. Merinov and W. A. Goddard, J Phys Chem C **116** (10), 6166-6173 (2012).
14. V. Tripkovic, E. Skulason, S. Siahrostami, J. K. Norskov and J. Rossmeisl, Electrochim Acta **55**, 7975-7981 (2010).

15. M. P. Hyman and J. W. Medlin, J Phys Chem C **111** (45), 17052-17060 (2007).
16. C. A. Menning, H. H. Hwu and J. G. G. Chen, J Phys Chem B **110** (31), 15471-15477 (2006).
17. H. Xin and S. Linic, J. Chem. Phys. **132**, 221101-221104 (2010).
18. P. Schultz, (SEQQUEST, Sandia National Laboratory).
19. A. Edwards, (SEQQUEST Post Analysis Code).
20. J. P. Perdew, K. Burke and M. Ernzerhof, Phys Rev Lett **77** (18), 3865-3868 (1996).
21. J. P. Perdew and A. Zunger, Phys Rev B **23** (10), 5048-5079 (1981).
22. G. Mills and H. Jonsson, Phys Rev Lett **72** (7), 1124-1127 (1994).
23. M. Peuckert and H. P. Bonzel, Surf Sci **145**, 230-259 (1984).
24. K. Bedürftig, S. Völkening, Y. Wang, J. Wintterlin, K. Jacobi and G. Ertl, J Chem Phys **111** (4), 11145-11154 (1999).
25. T. H. Rod, A. Logadottir and J. K. Norskov, J Chem Phys **112** (12), 5343-5347 (2000).
26. B. Hammer and J. K. Norskov, Surf Sci **343** (3), 211-220 (1995).
27. A. Ruban, B. Hammer, P. Stoltze, H. L. Skriver and J. K. Norskov, J Mol Catal A: Catal **115** (3), 421-429 (1997).
28. T. Hofmann, T. H. Yu, M. Folse, L. Weinhardt, M. Bar, Y. F. Zhang, B. V. Merinov, D. J. Myers, W. A. Goddard and C. Heske, J Phys Chem C **116** (45), 24016-24026 (2012).
29. V. R. Stamenkovic, B. Fowler, B. S. Mun, G. F. Wang, P. N. Ross, C. A. Lucas and N. M. Markovic, Science **315** (5811), 493-497 (2007).
30. J. Zhang, M. B. Vukmirovic, X. Ye, M. Mavrikakis and R. R. Adzic, Angew Chem Int Edit **44**, 2132-2135 (2005).
31. M. B. Vukmirovic, J. Zhang, K. Sasaki, A. U. Nilekar, F. Uribe, M. Mavrikakis and R. R. Adzic, Electrochim Acta **52** (6), 2257-2263 (2007).
32. M. K. Debe, Nature **486**, 43–51 (2012).
33. V. R. Stamenkovic, B. S. Mun, K. J. J. Mayrhofer, P. N. Ross and N. M. Markovic, J Am Chem Soc **128** (27), 8813-8819 (2006).
34. S. J. Kang, S. Lim, D. H. Peck, S. K. Kim, D. H. Jung, S. H. Hong, H. G. Jung and Y. S, International Journal of Hydrogen Energy **37**, 4685-4693 (2012).
35. H. C. Tsai, T. H. Yu, Y. Sha, B. Merinov, P. W. Wu, S. Y. Chen and W. A. Goddard, J Phys Chem C **118** (46), 26703-26712 (2014).
36. T. H. Yu, Y. Sha, B. V. Merinov and W. A. Goddard, J Phys Chem C **114** (26), 11527-11533 (2010).

FIGURES

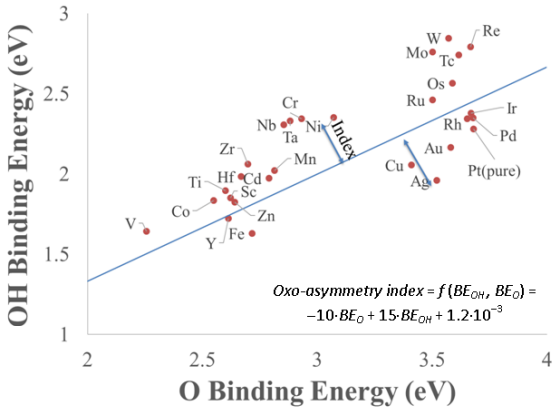

Figure 1. The OH binding energy vs. the O binding energy of the Pt-M-Pt sandwich catalysts The oxo-asymmetry index calculates the perpendicular distance of the Pt-M-Pt sandwich catalyst to the best fit oxo-symmetry line of the O and OH binding energies based on the data generated for a series of pure metals.[1] This index represents how well a given catalyst performs for process II (O → OH) of the ORR. A higher value of the oxo-asymmetry index represents strong OH binding and weak O binding. In this data set, Pt-W-Pt has the best index value, 6.97, and Pt-Ag-Pt shows the worst index value, –5.82. The oxo-symmetry line has an equation of $BE_{OH} = 0.667 \cdot BE_O - 8.17 \cdot 10^{-4}$.

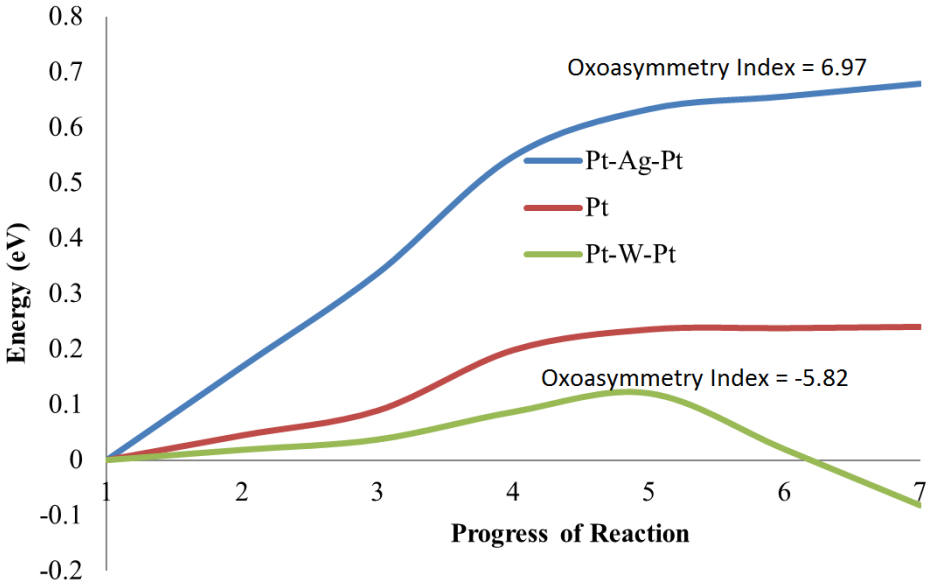

Figure 2. Energy barrier for the O hydration reaction on the best, Pt-W-Pt, and worst, Pt-Ag-Pt, sandwich catalysts.

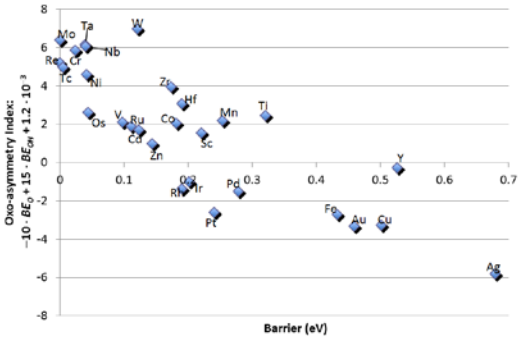

Figure 3. Energetic barrier of the O hydration reaction plotted versus the oxo-asymmetry index.

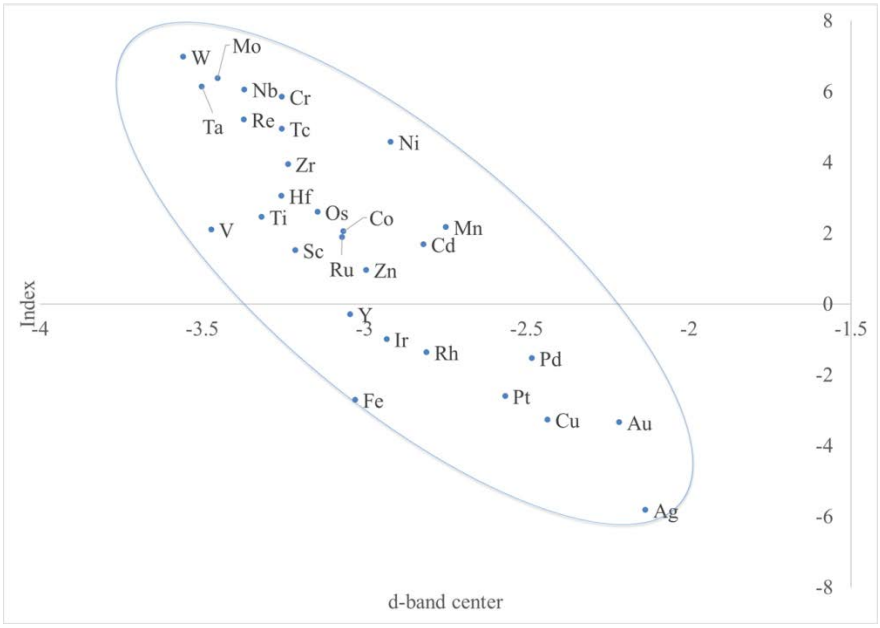
W
Mo
Nb
Cr
Ta
Re
Tc
Ni
Zr
Hf
Ti
Os
Co
Mn
V
Sc
Cd
Ru
Zn
Y
Ir
Rh
Pd
Fe
Pt
Cu
Au
Ag
Index
d-band center
8
6
4
2
0
-2
-4
-6
-8
-4
-3.5
-3
-2.5
-2
-1.5

a

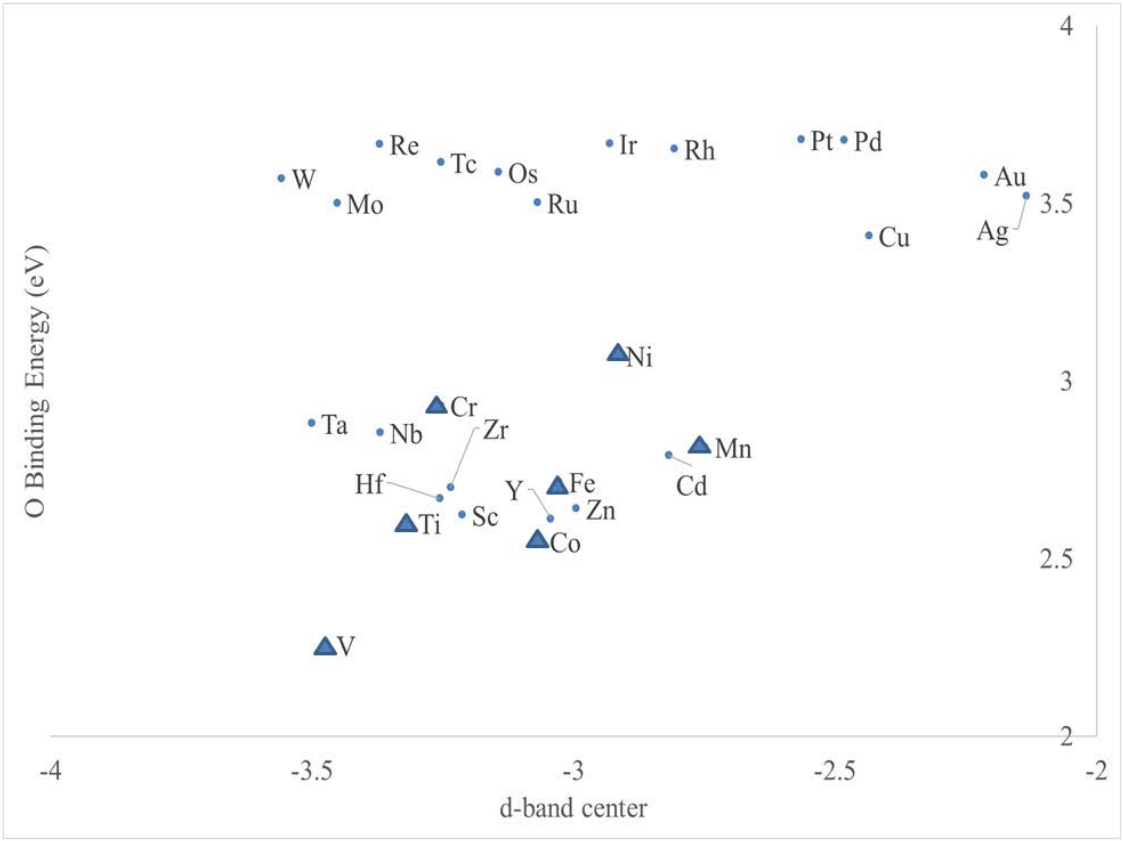
Re
Tc
Os
Ir
Rh
Pt
Pd
W
Mo
Ru
Au
Ag
Cu
Ni
Cr
Ta
Nb
Zr
Mn
Hf
Y
Fe
Cd
Ti
Sc
Zn
Co
V
O Binding Energy (eV)
d-band center
4
3.5
3
2.5
2
-4
-3.5
-3
-2.5
-2

b

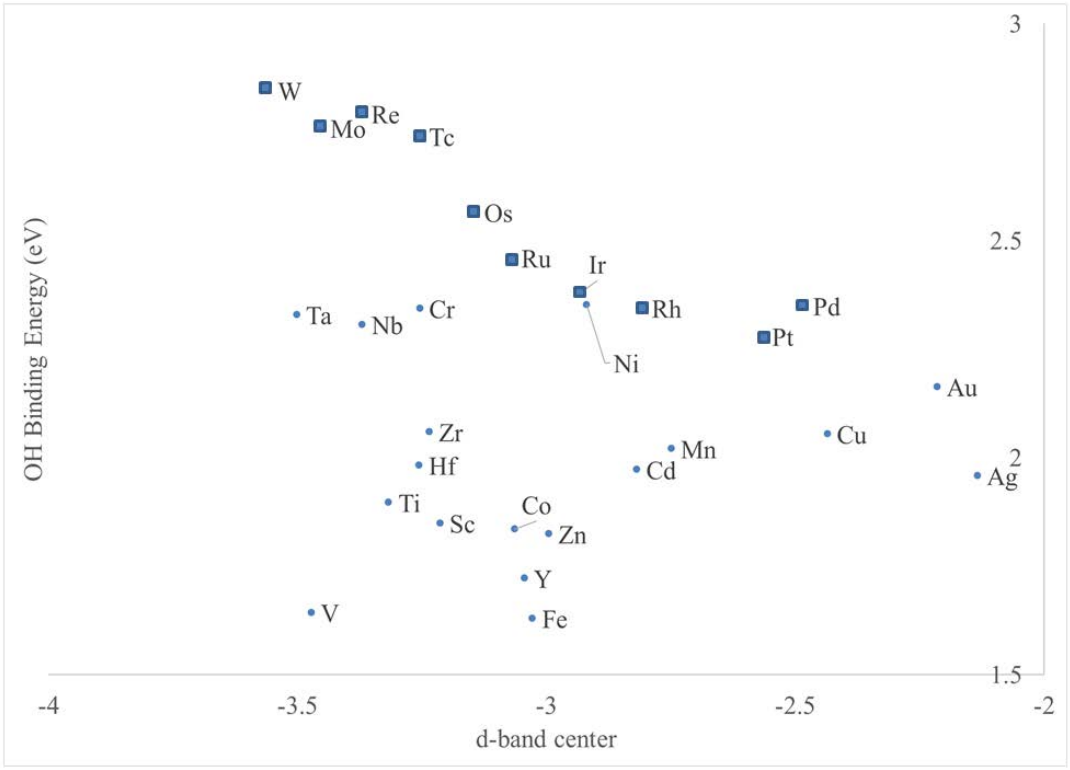

C

Figure 4. Plots of the index (a), O (b) and OH (c) binding energy vs. the d-band center. (b) The R^2 of the linear fit for O binding vs. d-band center improves from 0.1218 to 0.6521 when limiting the center metal from all transition metals to (Ti, V, Cr, Mn, Fe, Co, Ni, Pt)[16]. (c) The R^2 of the negative linear fit for OH binding vs. d-band center improves from 0.0541 to 0.8542 when limiting the center metal from all transition metals to (Mo, Tc, Ru, Rh, Pd, W, Re, Os, Ir, Pt)[17].

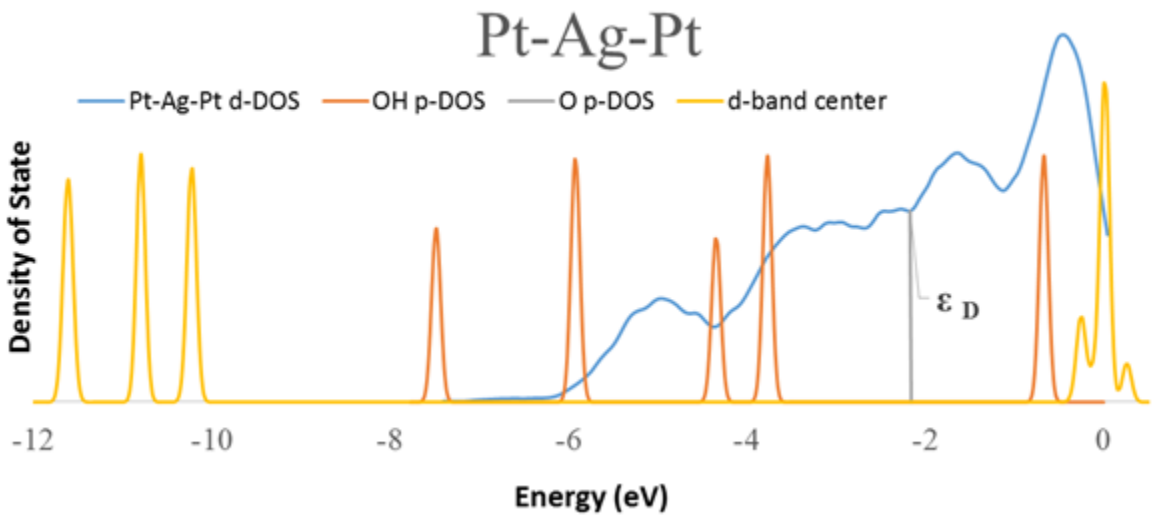

a

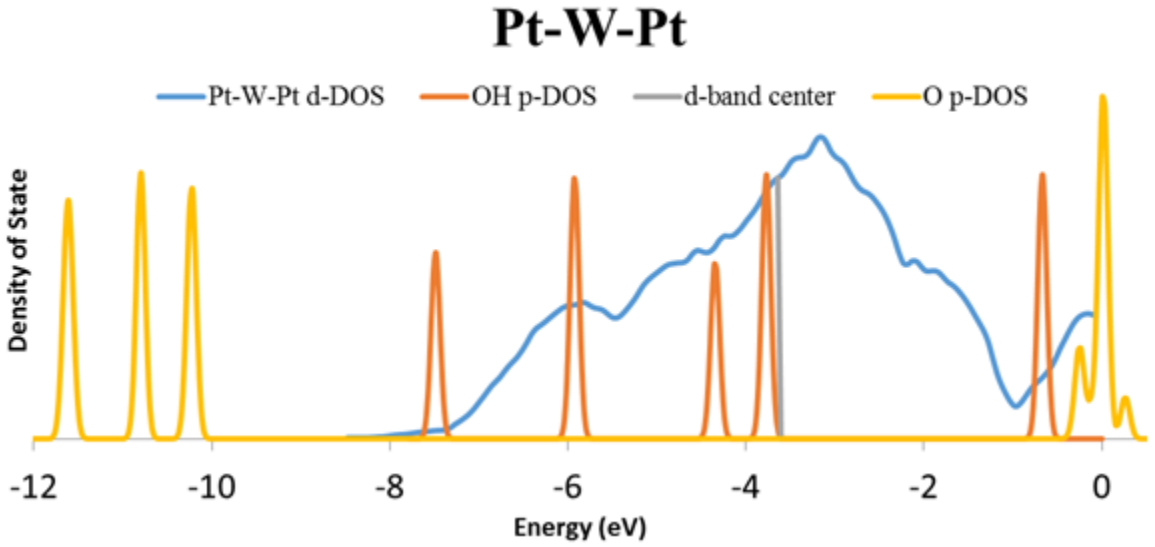

b

Figure 5. The d-DOS of Pt-W-Pt (a) and Pt-Ag-Pt (b). The p-DOS of atomic O is interposed showing three electrons: up-spin p_y, p_z, and p_x between –12 and –9 eV. The down-spin p_z lies near the Fermi level at 0 eV. The p-DOS of OH is interposed showing four electrons: up-spin p_y, down-spin p_y, up-spin p_x, and up-spin p_z, lie between –8 and –3 eV. The down-spin p_z lies near the Fermi level at 0 eV. The d-band center for Pt-W-Pt and Pt-Ag-Pt are –3.6 and 2.1 eV,

respectively. This analysis shows how the O hydration reaction is more favorable for the Pt-W-Pt, because its d-DOS overlaps better with the product, OH, p-DOS, while the d-DOS of the Pt-Ag-Pt overlaps better with the reactant, O, p-DOS.

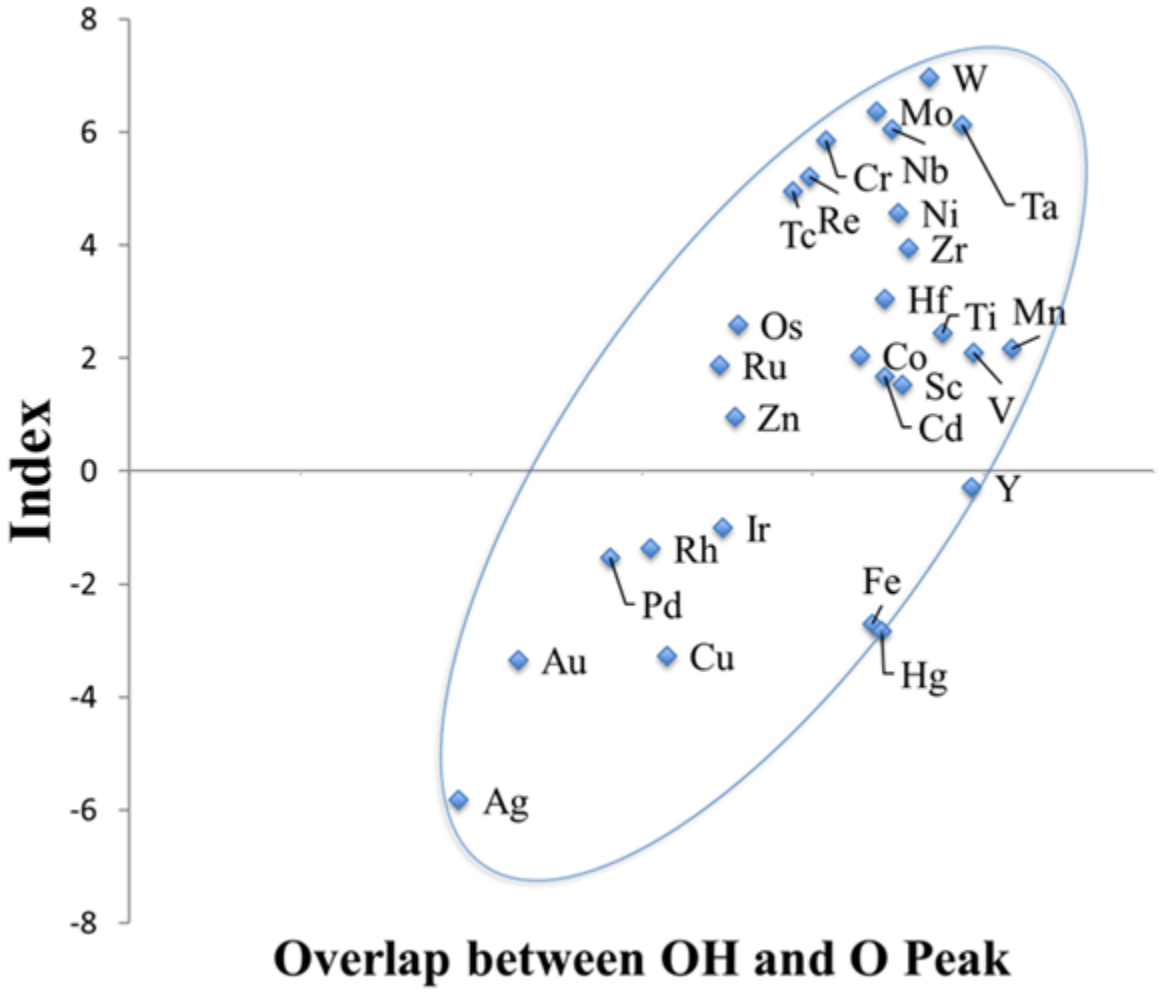

Figure 6. The overlap between the OH and O peaks plotted against the index for all 28 Pt-M-Pt calculations, where overlap = d-DOS(–5.93)+d-DOS(–4.35)+d-DOS(–3.77)+d-DOS(–0.67) –d-DOS(–0.27). The trend of the index vs. the overlap is universal and explains how data from the d-DOS can be extracted to understand how to improve reactions with correlated binding of the reactant and product.

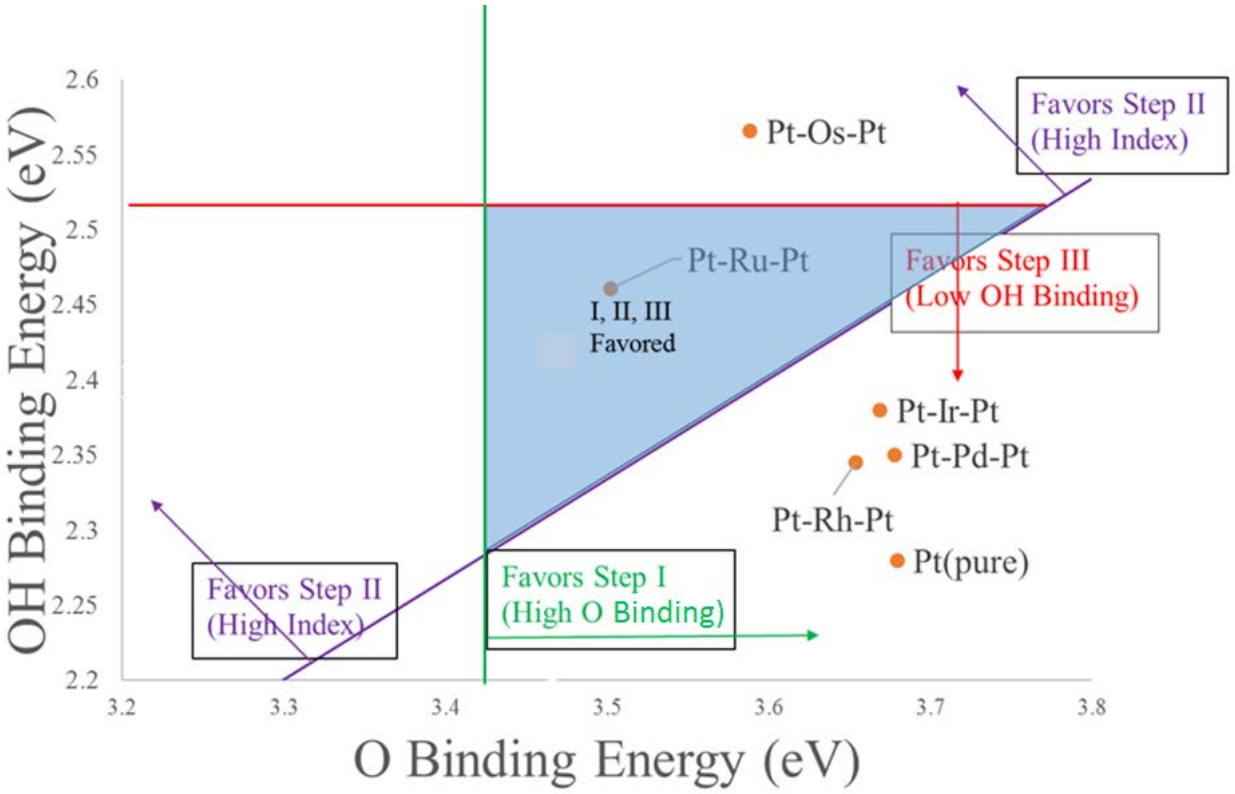

Figure 7. ORR preferences for the three steps of the ORR reaction as a function of O and OH binding energy: I) O_2 activation II) OH formation III) H_2O formation. The overall ORR is optimized in the triangle shown, where only Pt-Ru-Pt resides.

TABLES

Table 1. O and OH binding energies of Pt-M-Pt sandwiches.*

M	O Binding Energy (eV)	OH Binding Energy (eV)	Index
Sc	2.62	1.85	1.52
Ti	2.60	1.90	2.45
V	2.26	1.64	2.10
Cr	2.93	2.34	5.85
Mn	2.81	2.02	2.17
Fe	2.72	1.63	-2.71
Co	2.55	1.84	2.05
Ni	3.07	2.35	4.57
Cu	3.41	2.06	-3.27
Zn	2.64	1.82	0.96
Y	2.61	1.72	-0.29
Zr	2.70	2.06	3.95
Nb	2.85	2.31	6.06
Mo	3.50	2.76	6.37
Tc	3.62	2.74	4.95
Ru	3.50	2.46	1.88
Rh	3.65	2.35	-1.37
Pd	3.68	2.35	-1.53
Ag	3.52	1.96	-5.82
Cd	2.79	1.97	1.68
Hf	2.67	1.98	3.05
Ta	2.88	2.33	6.13

W	3.57	2.85	6.97
Re	3.67	2.79	5.21
Os	3.59	2.57	2.59
Ir	3.67	2.38	-1.00
Pt(pure)	3.68	2.28	-2.61
Au	3.58	2.16	-3.34

*Pt-Hg-Pt monolayer catalysts are unstable with oxygen adsorbates.

Table 2. Predicted Onset Potential of Pt-M-Pt sandwiches.* While the high index of Pt-W-Pt made the onset potential of $O + H^+ + e^- \rightarrow OH$ high, the strong binding to OH dropped the onset potential of the final reaction, $OH + H^+ + e^- \rightarrow H_2O$, to 0.55V. The recommended catalyst, Pt-Ru-Pt has a predicted onset of potential of 0.94 V.

M	$O + H^+ + e^- \rightarrow OH$	$OH + H^+ + e^- \rightarrow H_2O$	Predicted Onset Potential (eV)
Sc	1.53	1.55	1.53
Ti	1.60	1.50	1.50
V	1.68	1.76	1.68
Cr	1.71	1.06	1.06
Mn	1.51	1.38	1.38
Fe	1.21	1.77	1.21
Co	1.59	1.56	1.56
Ni	1.58	1.05	1.05
Cu	0.95	1.34	0.95
Zn	1.48	1.58	1.48
Y	1.41	1.68	1.41
Zr	1.66	1.34	1.34

Nb	1.76	1.09	1.09
Mo	1.56	0.64	0.64
Tc	1.42	0.66	0.66
Ru	1.26	0.94	0.94
Rh	1.00	1.05	1.00
Pd	0.97	1.05	0.97
Ag	0.74	1.44	0.74
Cd	1.48	1.43	1.43
Hf	1.61	1.42	1.42
Ta	1.75	1.07	1.07
W	1.58	0.55	0.55
Re	1.42	0.61	0.61
Os	1.28	0.83	0.83
Ir	1.01	1.02	1.01
Pt(pure)	0.90	1.12	0.90
Ag	0.88	1.24	0.88

*Pt-Hg-Pt monolayer catalysts are unstable with oxygen adsorbates.

TOC:

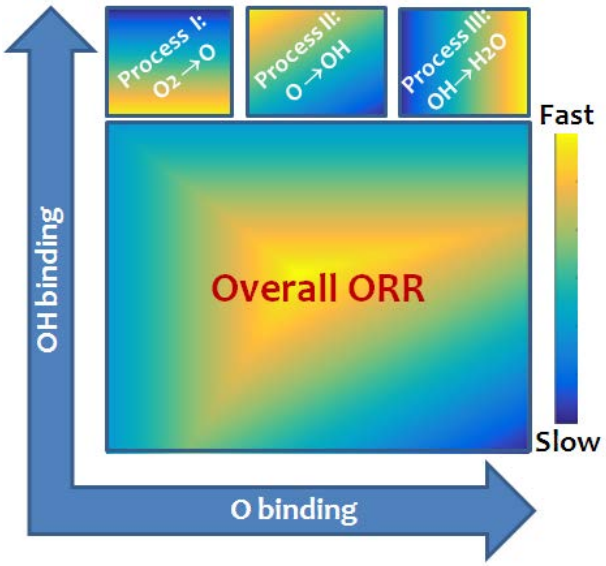
Process I:
O2→O
Process II:
O→OH
Process III:
OH→H2O
Fast
Overall ORR
Slow
OH binding
O binding